International Journal of Science and Research Archive
eISSN: 2582-8185
Cross Ref DOI: 10.30574/ijsra
Journal homepage: https://ijsra.net/

(RESEARCH ARTICLE)

Check for updates

Flow control for low-reynolds number airfoil performance enhancement using response surface methodology

Ndouba Ange Benai-dara *, ZhaoLin Chen and Leon Kaswango Kanama

College of Aerospace Engineering, Nanjing University of Aeronautics and Astronautics, Nanjing 210016, China.

International Journal of Science and Research Archive, 2024, 13(02), 3019-3029

Publication history: Received on 10 November 2024; revised on 18 December 2024; accepted on 20 December 2024

Article DOI: https://doi.org/10.30574/ijsra.2024.13.2.2545

Abstract

Low Reynolds number flows are characterized by boundary layer separation due to the effect of viscous forces. The separated flow may reattach through the exchange between the molecules resulting in Laminar Separation Bubble LSB. LSB, known for its detrimental effect on the performance is sensitive to the airfoil geometry. The current paper describes the use of trip boundary on the suction surface of SD7003 airfoil as flow control technique to enhance the airfoil performance at $Re = 6 \times 10^4$ and $\alpha = 4deg$ using numerical analysis. Due to the complexity of finding the trip size and location, Response Surface Methodology RSM is used to obtain the optimum combinations between the height, width and the position of the turbulator. Thus, the design variables are the height [0.2mm,0.6mm], width [140mm, 200mm] and the position of the trip away from the leading edge [10%c, 25%c]. Using the Desirability approach with Nelder-Mead simplex algorithm, the trip location is found to be effective downstream the separation location of the untripped airfoil. At the optimum design parameters, the length of LSB has decreased by 2.32% and the airfoil performance increased by 6%.

Keywords: Low-Reynolds Number; Laminar Separation Bubbles; SD7003 Airfoil; Trip Turbulator; Response Surface Methodology; Airfoil Performance

1. Introduction

The low Reynolds number regime has become a field of great interest with the advent of Unmanned Aerial Vehicles UAV and Micro Aerial Vehicles MAV. The boundary layer of the airfoils operating at this regime does not carry sufficient momentum and as result, the laminar boundary layer separates when encountering a strong adverse pressure gradient [1-3]. If the momentum at the boundary layer is further weak, the layer remains separated while transition occurs late causing a large periodic shedding. The separated boundary layer can incept Kelvin-Helmholtz vortices into the shear layer which break down into small turbulent spots resulting in reattachment to transition to turbulent flow and thus creating LSB. Due to its direct effect on the airfoil's performance, LSB is intensively studied [4-6]. Several studies have shown that the length of LSB is sensitive to flow conditions. For instance, an increase in angle of attack or Reynolds numbers decrease the size of LSBs or even burst completely and a change in the airfoil geometry affects the variation of lift and the separation point.

With the advent of high-power computers, the low Reynolds number flow around an airfoil can be duplicated and computed with accuracy. The flow features that are Separation, Transition and Reattachment can be tracked and the performance of airfoils can be known at various conditions. This numerical method known as Computational Fluid Dynamics CFD is based on the Navier-Stokes equations which need to be converted into algebraic equations by a model. Models such as Direct Numerical Simulation DNS and Large Eddy Simulation LES prove to be reliable in capturing the transition from laminar to turbulent; However, these models are both time-consuming and costly [7]. Other models less costly such Reynolds-Averaged Navier-Stokes models are being used providing satisfactory results. Catalano and

* Corresponding author: Ndouba Ange Benai-dara

Tognaccini [8] used the RANS model $k-\omega\ SST$ to predict the flow features around SD7003 airfoil at Reynolds number of $Re = 6 \times 10^4$ and found the model to show an accuracy close to LES [9] and Implicit LES [10] in predicting the separation, transition and reattachment point and the pressure coefficient.

The flow separation at low Reynolds number reduces the effective camber and increases the pressure drag thereby decreasing the airfoil performance. In order to decrease the pressure drag, researchers employed one of these two techniques [11-15]. The first technique is to carefully tailor the pressure distribution around the airfoil to permit an early transition. This method is well understood, requiring the experience of the designer. The second is the use of turbulators such as vortex generators, trip, zigzag turbulator etc. to change the nature of the flow downstream the separation point by creating streamwise vortices leading to turbulent flow. Even though turbulators have been used for over 50 years in the aircraft industry, the principle behind is scarcely understood as one configuration of the turbulator on an airfoil may not be effective on another airfoil [16]. In the early stage of this study, a feasibility analysis is conducted as to which of the turbulator can be used on SD7003 airfoil to enhance the performance. The analysis has led to a choice between vortex generators and trips. Mwenegoha and Jabbal [17] employed the vortex generators and the zigzag turbulator on the wing of a Skyranger Microlight aircraft to enhance the performance and the stall angle. It was found that vortex generators increase slightly the performance only at high angles of attack. Huber and Mueller [18] studied the effect of trip wire roughness on the performance of the Wortmann FX 63-137 airfoil at Reynolds number of $Re = 1 \times 10^5$. And it was found that when the trip is located at the maximum thickness of the airfoil at $\alpha = 4°$, the performance increases by 3%. Lyon et al. [19] tested three categories of boundary layer trips (single 2D, multiple 2D and 3D trips) on three airfoils at low angles of attack over the Reynolds numbers of 1×10^5 to 3×10^5 and their findings show little advantages in utilizing multiple 2D or 3D trips over the single 2D trip and the single trip is more effective for short LSB. Therefore, based on the advantages of trip and the short laminar separation bubble displayed by SD7003 airfoil at low angles of attack, the trip turbulator is selected and applied on the airfoil (see Figure 1).

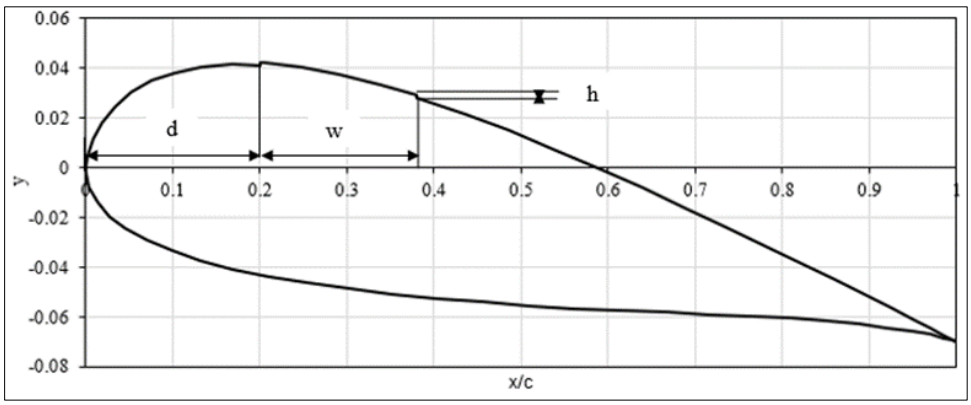

Figure 1 Trip turbulator applied to SD 7003 at α=4deg (d stands for the distance away from LE, h and w are the height and width respectively).

The application of the trip geometry on an airfoil is characterized by the trip height, width and its location away from the leading edge. Part of the difficulty of the trip application mentioned by Lyon et al. [19] is the finding of the optimum design variables which can increase the lift and decrease the drag. Response Surface Methodology RSM, known for its effectiveness in finding the optimum combinations can be used to alleviate this difficulty. RSM allows a random selection of the design variables and does not require the calculations of the local sensitivity of each variable [20, 21]. Furthermore, the method can smooth the high frequency noise of the objective function thus becoming more effective for optimization problems. Oh [22] used the two prominent surrogate models, Response Surface Methodology RSM and Artificial Neural Network ANN to optimize a transonic airfoil and found that at the low degree of freedom, RSM exhibits superiority compared to ANN. Landman et al. [23] utilized RSM to find the optimum combinations of the trip factors namely the distance from the leading edge, width and thickness to enhance the performance of low Reynolds number propeller.

In this current study, the Faced Central Composite Design FCCD-RSM [24] combined with High-Fidelity using $k-\omega\ SST$ model is used to optimize the design variables of the trip configuration at $Re = 6 \times 10^4$ and $\alpha = 4°$. The Selig-Donovan SD7003 airfoil is selected due to availability of the experimental and numerical data [9, 10]. It is expected that the use of the trip will enhance the aerodynamics performance by delaying the onset separation.

2. Numerical Method

The current flow is incompressible as the density variation with time is insignificant. The Navier-Stokes equations are utilized to describe the flow pattern in the finite control volume. Ignoring the effect of body forces, the continuity, momentum equations are respectively given as:

$$\frac{\partial}{\partial t}\iiint_v \rho \, dv + \iint_S \rho V . dS = 0 \qquad \ldots\ldots\ldots\ldots\ldots (1)$$

$$\frac{\partial}{\partial t}\iiint_v \rho V \, dv + \oiint_S (\rho V . dS) V = -\oiint_S p \, ds + F_{viscous} \qquad \ldots\ldots\ldots\ldots\ldots\ldots (2)$$

Where ρ is the fluid density, V and p are the freestream velocity and the pressure.

The flow simulation in this study is around an airfoil at low-Reynolds number where the wake region and free shear region need to be taken into account to accurately predict the aerodynamic characteristics. Wilcox [25] developed a model $k-\omega$ which allows the treatment of rough walls and surface mass injection. The parameters k and ω stand for turbulent kinetic energy and specific dissipation rate respectively. Unlike other two transport equation models, $k-\omega$ doesn't incorporate the damping function into the formulation and allows Dirichlet boundary conditions by setting numerical value of variables at the boundary conditions. However, the model fails to account for the flow features in the wake region of the boundary layer due to the strong sensitivity to the freestream dissipation rate outside the boundary layer [26]. In the wake region, $k-\varepsilon$ model is preferred. Menter [26] introduced an improved version of $k-\omega$ model to effectively capture flow features both in sublayer and logarithmic region of the boundary layer and wake region. The idea behind the model was to utilize the original $k-\omega$ in the inner region of the boundary layer and to switch on to the standard $k-\varepsilon$ in the wake region. In order to achieve this, the two transport equations of the original $k-\omega$ and those of $k-\varepsilon$ model were multiplied by F_1 and $(1-F_1)$ respectively. The combination of these equations results in two transport equations given as follows:

$$\frac{\partial(\rho k)}{\partial t} + \frac{\partial(\rho k u_j)}{\partial x_j} = \tau_{ij}\frac{\partial u_i}{\partial x_j} - \beta^*\rho\omega k + \frac{\partial}{\partial x_j}\left[(\mu + \sigma_k\mu_t)\frac{\partial k}{\partial x_j}\right] \qquad \ldots\ldots\ldots\ldots (3)$$

$$\frac{\partial(\rho\omega)}{\partial t} + \frac{\partial(\rho\omega u_j)}{\partial x_j} = \gamma\frac{\rho}{\mu_t}\tau_{ij}\frac{\partial u_i}{\partial x_j} - \beta\rho\omega^2 + \frac{\partial}{\partial x_j}\left[(\mu + \sigma_\omega\mu_t)\frac{\partial\omega}{\partial x_j}\right] + 2(1-F_1)\rho\sigma_{\omega_2}\frac{1}{\omega}\frac{\partial k}{\partial x_j}\frac{\partial\omega}{\partial x_j} \qquad \ldots\ldots\ldots (4)$$

Where β^*, β, γ, σ_k, σ_ω and σ_{ω_2} are constants given in [26], τ_{ij} is the Reynolds stress tensor and F_1 is the blending function which takes the value of 1 in the inner region and 0 in the wake region.

$k-\omega$ model in this study is combined with the shear stress transport SST to account for the eddy viscosity in the adverse pressure gradient region resulting in four transport equations.

2.1.1. Verification of Numerical Method

High-fidelity solver Fluent is utilized to assess the numerical method at Reynolds number of $\mathrm{Re} = 6 \times 10^4$, angle of attack of $\alpha = 4deg$ and turbulence intensity of $\mathrm{Tu}_\infty = 0.1\%$. The solver is based on the integral form of the governing equations which guarantees the conservation laws and avoiding non-differential jump. SD7003, a well-known low-Reynolds number airfoil for which experimental and numerical data are available is selected [9, 10, 27]. The chord length of the airfoil is 1m. Counsil and Boulama [28] studied the effect of the computational domain on the flow features. Two domains of 10c and 20c upstream the airfoil were considered. For both configurations, the far-field downstream of the airfoil was 20c. It was found that the domain of 20c upstream the airfoil was independent of the separation and reattachment points. Thus, the current computational domain is designed after their configuration as shown in Figure 2.

Besides the effect of the computational domain, numerical results depend on the grid density. A total of 6 grids with C-H typology centered around the airfoil were considered (see Table 1). Case 1 is coarsely generated and the remaining cases are generated by refining case 1 either streamwise or normal wise. The height of the first cell distance for all the cases is obtained by setting a y^+ less than 1. All the simulations were computed using SIMPLE scheme for pressure-velocity coupling with the second order scheme and to avoid truncation errors, double precision is used.

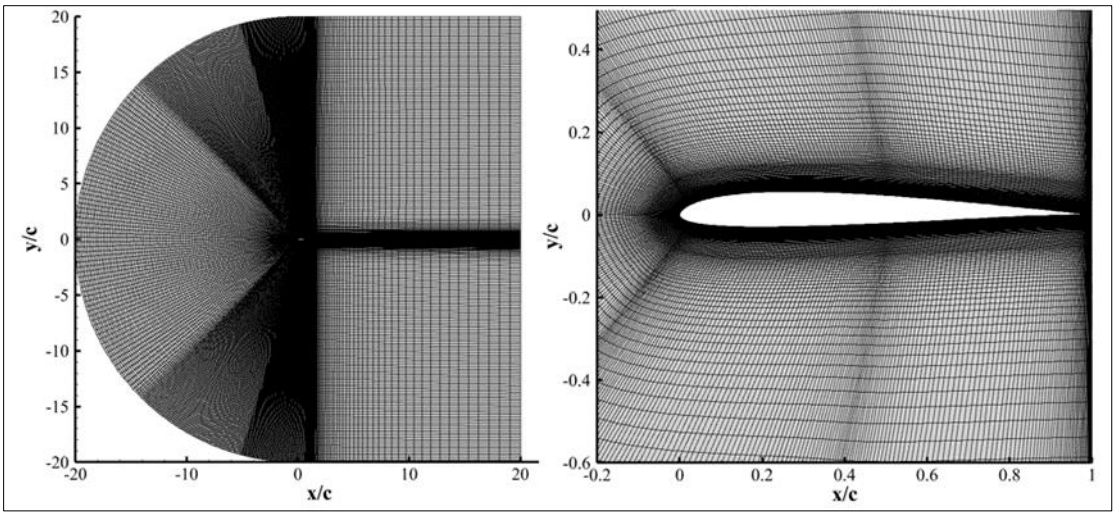

Figure 2 Computational domain and grid typology for SD7003 airfoil.

The flow features are characterized by separation point S, transition point T, reattachment point R and the length of the LSB relative to the chord. These are obtained from the plots of the friction coefficient C_f and verified with the pressure coefficient C_p on the upper surface of the airfoil. For instance, the separation point is marked by the crossing of the x-axis by the C_f plot in the negative y-axis. The sudden decrease of the curve until reaching its negative peak indicates the transition point. And the reattachment point is specified as the abrupt recovery from its negative peak to a positive value. The length of the LSB is then calculated as the difference between the reattachment point and the separation point. As for C_p plot, the separation poin**t** is estimated as the intersection of nearly linear pressure recovery region to the nearly constant-pressure region. And the transition and reattachment points are the local maximum and minimum of the second derivative of the polynomial fit respectively [29]. Table 1 summarizes the flow features obtained by RANS model $k-\omega\ SST$ for the considered grid densities. The increase of grid in streamwise and normal wise has no effect on the separation point; the point remains unchanged. Likewise, the transition point is somewhat constant for all cases. On the contrary, the reattachment point varies as a function of grid densities in both streamwise and normal wise. When the grid is increased in the normal direction, the reattachment decreases slowly whereas the increase in the streamwise decreases suddenly the reattachment point. The cases 4 to 6 displayed a short and consistent LSB length compared to cases 1 to 3. In comparison to available computational and experimental data (see Table 2) and considering the computational time, Case 4 is chosen for the remaining study.

Table 1 Grid sensitivity study on SD7003 at $\boldsymbol{Re = 6.0 \times 10^4}$, α =4deg and $\mathbf{Tu_\infty = 0.1\%}$.

Case	R_{inlet}/c	Grid density	x_{sep}/c	x_{trans}/c	x_{reat}/c	L_{LSB}/c
1	20	456x135	0.20	0.57	0.72	0.52
2	20	456x190	0.20	0.57	0.70	0.50
3	20	456x245	0.20	0.56	0.69	0.49
4	20	640x190	0.20	0.56	0.64	0.44
5	20	640x245	0.20	0.56	0.65	0.45
6	20	900x245	0.20	0.57	0.64	0.44

Figure 2 displays the friction and pressure coefficient plots for RANS model $k-\omega\ SST$ compared with Large Eddy Simulation LES [9] and Implicit Large Eddy Simulation ILES [10]. Based on C_f plot, the separation and reattachment points predicted by RANS are in agreement with LES and ILES. However, the model predicts an earlier transition. As for the pressure coefficient, no significant difference is observed between RANS model and LES. Due to the satisfactory agreement between the published data and the current results, $k-\omega\ SST$ model is sufficient to evaluate the aerodynamics performance of SD7003 airfoil at $Re = 6 \times 10^4$ and angles of attack range of $\alpha = [0deg, 8deg]$.

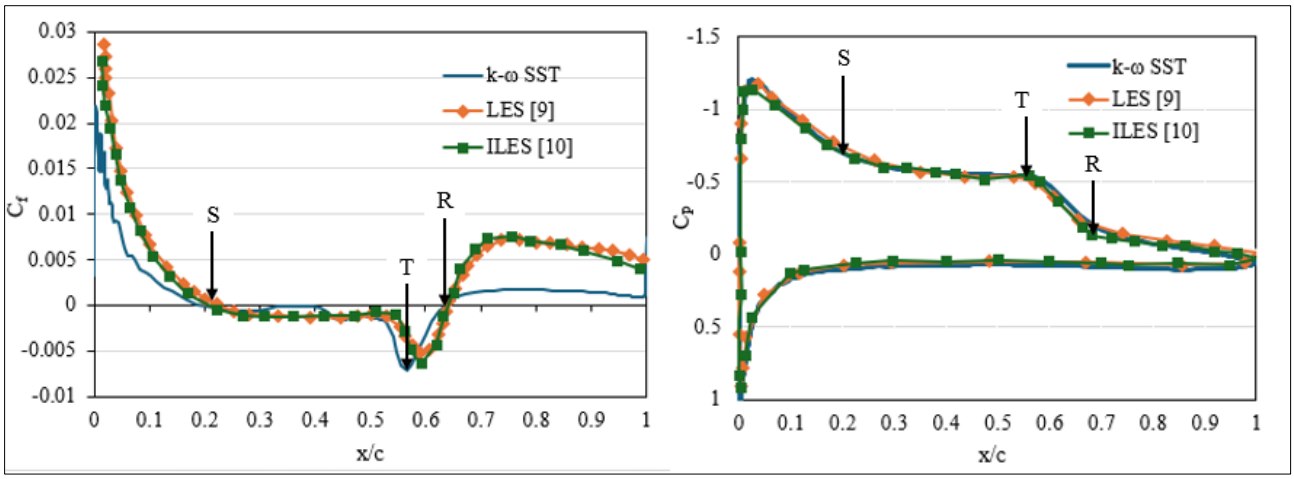

Figure 3 Friction and pressure coefficient distribution over SD7003 airfoil for Grid 4

Table 2 Time-averaged LSB characteristics: SD7003 at $\boldsymbol{Re = 6.0 \times 10^4}$ and $\boldsymbol{Tu_\infty = 0.1\%}$.

AoA, deg	Method	x_{sep}/c	x_{trans}/c	x_{reat}/c	L_{LSB}/c
4	2-D $k-\omega$-SST	0.20	0.60	0.70	0.50
	3-D LES [9]	0.25	0.52	0.61	44
	3-D ILES [10]	0.23	0.55	0.65	0.42
	Wind tunnel [3]	0.30	0.53	0.62	0.32

The airfoil efficiency defined as the ratio of the lift coefficient to the drag coefficient is shown in Figure 4. The results predicted by the RANS model $k-\omega\ SST$ are compared with those of experiment [3] and ILES [10] for angle of attack range of [0deg, 8deg]. Over this angle of attack range, $k-\omega\ SST$ underpredicted the aerodynamics efficiency compared to both ILES and the experiment. However, as angle of attack increases, the error difference between the experiment and RANS decreases. The error difference between the experiment and $k-\omega\ SST$ model for all the considered angles of attack is less than 25%. The residuals at $\alpha = 4deg$ is below 10^{-5} as shown in Figure 4. Since the aim of this study is to show the effectiveness of trip in performance enhancement, this result is accounted for as acceptable.

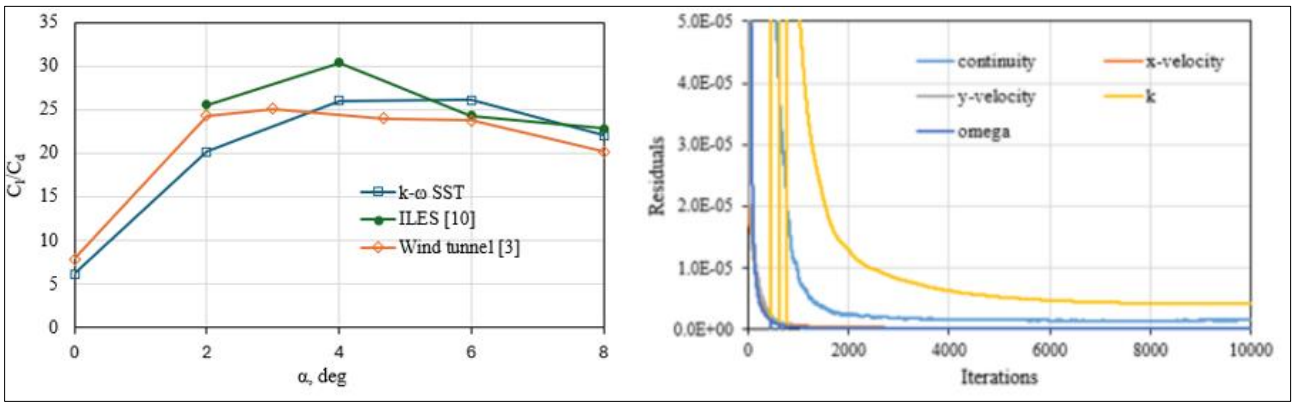

Figure 4 Lift-to-drag ratio compared with available data at $Re = 6.0 \times 10^4$ and $Tu_\infty = 0.1\%$ and the residuals at $\alpha = 4deg$

3. Response Surface Methodology

3.1. Overview

The overall procedure of RSM is shown in Figure 5. As any optimization approaches, RSM starts by identifying the design parameters affecting the objective function. Each parameter has a lower and upper bound value to maximize the value of the objective function. Moreover, the Design of Experimental is used to select the number of experimental combinations which are computed for the response function. Then, a response surface is established to obtain the mathematical model. The first order model is largely sufficient when the relation between the design variables and the response is linear. However, most design problems including the current study expect the effect of the interaction between the design variables and the two-factor interaction 2FI general formulation is given as:

$$y = \beta_0 + \sum_{i=1}^{k} \beta_i x_i + \sum_{i=1}^{k} \sum_{j=2_{i<j}}^{k} \beta_{ij} x_i x_j + \varepsilon \quad \ldots\ldots\ldots \quad (5)$$

Where y is the response function, x_i and x_j are design variables, β_0 the intercept coefficient, β_i the coefficient of design variable x_i, β_{ij} the coefficient of the interaction of x_i and x_j for j=1,2,...,k and $i < j$ and ε is the random error normally distributed with the mean θ and the standard deviation σ.

To ensure the adaptability of the model and that the built model reflects the optimization target, the deterministic factor R^2 is used and given as:

$$R^2 = 1 - \frac{SS_E}{SS_T} \qquad \ldots\ldots\ldots\ldots \quad (6)$$

Where SS_E and SS_T are the sum of squared residuals and total sum of squares respectively. The value of R^2 is between 0 and 1. When R^2 is close to 1, the model has a high reference value which is preferred and when it is close to 0, the reference value is low. Finally, the Desirability approach with Nelder-Mead simplex algorithm is used to obtain the final optimal point within the design space.

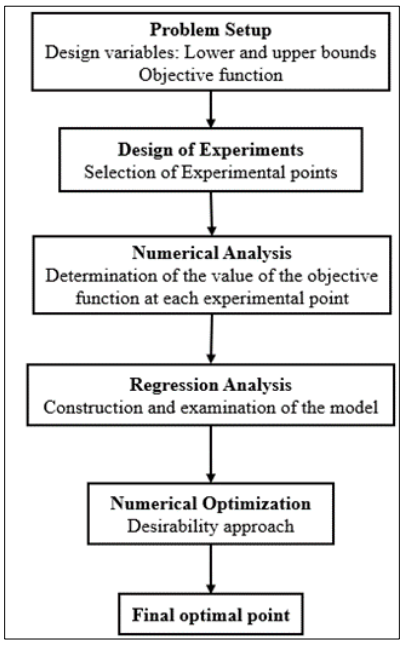

Figure 5 Optimization procedure using RSM.

3.2. Design variables and Objective Function

The application of trip on an airfoil is characterized by its height, width and location from the leading edge [18, 19]. The height of the trip k is found by Huber and Mueller (1987) to be a function of the external velocity U_e and kinematic viscosity ν and given as:

$$k = \frac{826\nu}{U_e}\exp(-0.9\Lambda_1) \quad \text{..... (6)}$$

Where Λ_1 is a non-dimensional pressure gradient term estimated to be between 0 and 0.3. Thus, the range of k used in this study is [0.2mm, 0.6mm].

As for the trip width, its range is selected based on the trip width used by Lyon et al. [19]. From the numerical analysis, the separation point occurs at 20% of chord and the trip location range away from the leading edge is selected to be upstream and downstream the separation point. The three design parameters and the range of their levels are shown in Table 3 which Design-Expert DX software [30] needs to provide various combinations. The aim of these combinations is to obtain the optimum design variables which maximize the airfoil performance given by:

$$E = \frac{C_l}{C_d} \quad \text{.....(7)}$$

Where C_l and C_d are airfoil lift and drag coefficient respectively.

Table 3 Design parameters and their range.

Factor	Unit	Low	High
Height	mm	0.2	0.6
Depth	mm	140	200
Distance from LE	%c	10	25

4. Results

The Response Surface Methodology provides a comprehensive approach to experiment analysis including significance testing, model building and adequacy. The ANOVA table of the airfoil performance E is shown in Table 4. The P-value of the model is less than 0.0001 which indicates that the model is significant. P-value is a metric used to show the significancy of a model or variable. When the P-value of a variable is less than 0.05, the parameter is said to be significant; Otherwise, it is not. The variables A (trip height) and C (trip width) are significant whereas variable C (trip location from leading edge) is insignificant. However, its interaction with variables A and B is significant. The mathematical model of the airfoil performance E in terms of coded factors (A: trip height; B: trip width and C: trip location) is given by:

$$E = 23.9334 + 0.03264A - 0.040274B + 0.050807C + 0.06104AB + 0.11544AC - 0.086200BC \text{ ..... (8)}$$

From the signs of the equation above, the variable B and the interaction between B and C have a negative effect whereas the variables A, C and the interactions between A and B, A and C have a positive effect on the performance.

Table 4 ANOVA for the performance E.

Source	Sum of Squares	df	F-value	P-value
Model	0.2486	6	3.84	< 0.0001
A-h	0.0107	1	0.9889	0.0079
B-w	0.0162	1	1.51	0.0414
C-d	0.0258	1	2.40	0.1982
AB	0.0298	1	2.77	0.1700
AC	0.1066	1	9.89	0.0214
BC	0.0594	1	5.52	0.0146
Residual	0.1401	13		
Cor Total	0.3886	19		

Table 5 summarizes the fit statistics of the model. The correlation factors R^2, adjusted R^2 and predicted R^2 were high within the range [0,1] and the difference between adjusted R^2 and predicted R^2 was less than 0.2. The considered model could explain 82.91% of the variation seen in efficiency response.

Table 5 Fit statistics for aerodynamics performance E

Parameter	Value
R^2	0.8291
Adjusted R^2	0.8072
Adjusted R^2	0.6945

To have a valid and reliable response model, criteria such as normality and independent distribution needed to be verified. The normality and independent distribution assumptions are visualized through the plot of normal probability and residuals versus predicted values respectively. During the normality evaluation, the residuals are expected to follow the straight line in the normal probability plot. If the lack of normality exists, the residuals form an S/I-shaped curve. As it can be seen in Figure 6(a), the residuals follow the straight line and therefore the normality criterion is not violated. And for the independent distribution assumption, the residuals are expected to be randomly scattered which is the case in Figure 6(b). Therefore, this model is reliable and can be used to carry out numerical optimization.

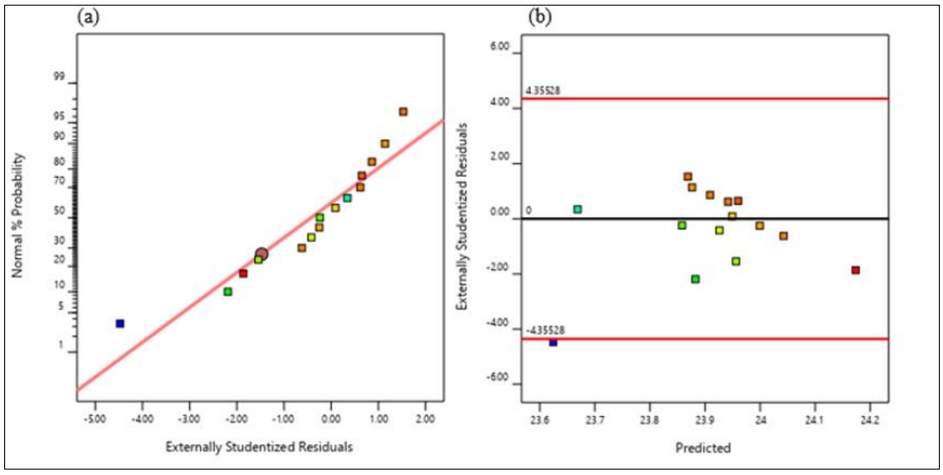

Figure 6 Normal Probability (a) and Residuals vs Predicted E values (b)

The ultimate goal of the Response Surface Methodology is to determine the optimum values that maximize the response. However, the optimization problem becomes difficult when more than one response is considered for it requires satisfying all the response criteria. Derringer and Suich [31] introduced within RSM a technique in which multi-response problem is reduced to single-response problem known as Desirability function. The lift and drag coefficient and the ratio lift-to-drag are the responses in the airfoil optimization. Based on the regression model results, the numerical optimization is performed to obtain the variables which affect the efficiency distribution where C_l is maximized and C_d minimized. The desirability approach with the Nelder-Mead Simplex direct search algorithm in Design Expert software [30] is used for this purpose. The optimum combinations along with the predicted C_l, C_d and E and computed E are summarized in Table 6. The optimum location of the trip is found to be at 25% of chord, behind the separation point of the airfoil without the trip. The computed result is in good agreement with the predicted value with an error of less than 1%.

At low Reynolds number, the drag due to flow separation (pressure drag) is the major component of the total drag and a decrease of the pressure drag by delaying the onset separation will result in airfoil performance enhancement. Figure 7 shows the flow features (separation, transition and reattachment) of SD7003 airfoil without and with trip. The flow separation of the airfoil with trip occurs at 22% of chord which is delayed compared to the airfoil without the trip. Moreover, the trip has delayed the reattachment point resulting in a slight shortening of the Laminar Separation Bubble. As a result, the airfoil performance has increased by 6%.

Table 6 Numerical optimization goals and Fluent solver compared to the predicted value.

Factor	Goal	Optimum Value	Predicted E	Computed E
A: L_2, mm	In Range	0.6	24.178	24.242
B: L_3, mm	In Range	195.568		
C: L_4, %c	In Range	25		
C_l	Maximize	0.580		
C_d	Minimize	0.024		

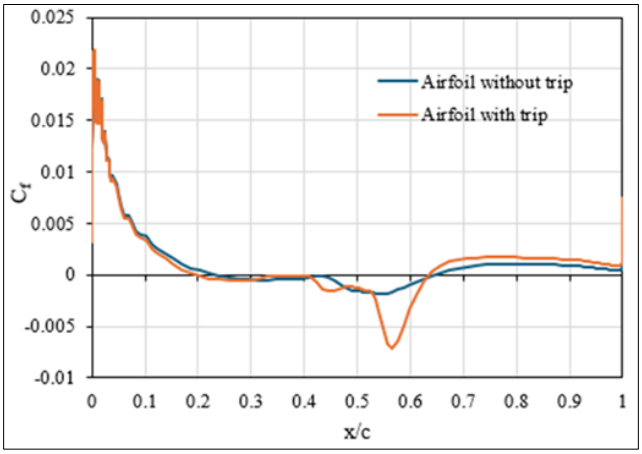

Figure 7 Friction coefficient of the upper surface of the airfoil without and with trip

Table 7 Flow features and Airfoil performance with and without trip.

Airfoil	x_{sep}/c	x_{reat}/c	L_{LSB}/c	Performance E
Original	0.20	0.64	0.44	22.761
Tripped	0.22	0.65	0.43	24.387
Error, %	9	1.56	2.32	6.04

Figure 8 displays the pressure and velocity contours around the airfoil with the trip. The stagnation point is observed to occur at the airfoil leading edge and the pressure is equally distributed on the upper and lower surfaces. Notice that the pressure over the upper surface is negative which in return results in high velocity thus confirming Bernoulli's principle. The use of trip creates low pressure zone prior to its location which results in performance enhancement.

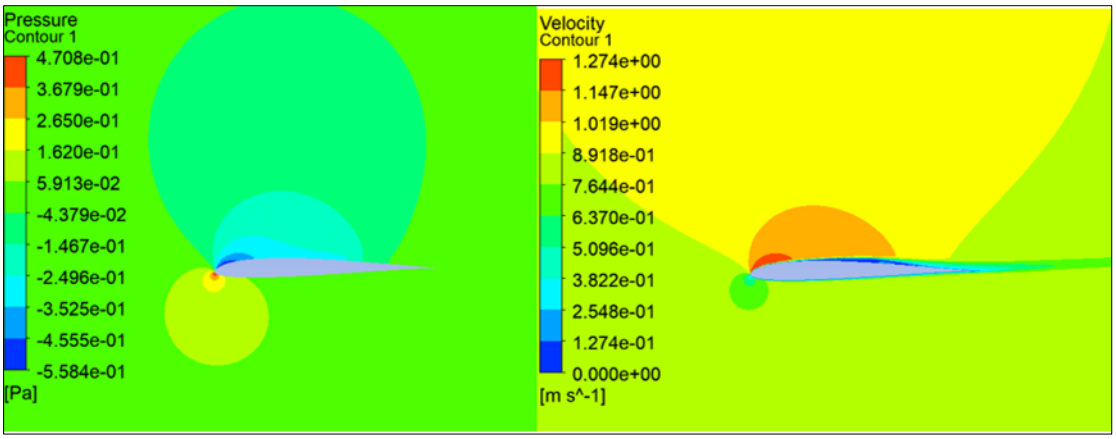

Figure 8 Pressure and velocity contour around the tripped airfoil

5. Conclusions

The drag component due to flow separation is the major component increasing the total drag at low Reynolds number regime. Decreasing this component is beneficial for the overall performance of the airfoil. The current study utilized trip turbulator to enhance the performance of SD7003 airfoil at Reynolds number of $Re = 6 \times 10^4$ and angle of attack of $\alpha = 4deg$. In addition, the surrogate model Response Surface Methodology RSM within Design-Expert software was used to obtain the optimum location of the trip away from leading edge and the trip height and width. The optimum trip location was found to be downstream the separation point of the airfoil without the trip and the separation and reattachment points of the airfoil with the trip were delayed. Finally, the length of Laminar Separation Bubble has decreased by 2.32% and the tripped airfoil performance increased by 6%.

Compliance with ethical standards

Disclosure of conflict of interest

Authors declare no conflict of interest.

Funding

The author(s) disclosed receipt of the following ffnancial support for the research, authorship, and/or publication of this article. The present work is supported by the National Natural Science Foundation of China under Grant No. 12002161, 12032011, and the National Key Laboratory of Helicopter Aeromechanics, Funding No. 2023-HA-LB-067-06.

References

[1] Carmichael, B. H. Low reynolds number airfoil survey—Vol. 1. NASA CR-165803, 1981. https://ntrs.nasa.gov/api/citations/19820006186/downloads/19820006186.pdf

[2] Lin, J. C. M., & Pauley, L. L. Low-reynolds-number separation on an airfoil. AIAA Journal, Vol. 34, No. 8, 1996, pp. 1570–1577. doi:10.2514/3.13273. https://doi.org/10.2514/3.13273

[3] Selig, M. S., Donovan, J. F., & Fraser, D. B. Airfoils at low speeds, soarTech Publications, Virginia Beach, VA.

[4] Aono H., Nonomura T., Anyoji M. A numerical study of the effects of airfoil shape on low Reynolds number aerodynamics. Proceedings of the 8th International Conference on Engineering Computational Technology. 2012.

[5] McGranahan, B. D., & Selig, M. S. Surface oil flow measurements on several airfoils at low reynolds numbers. AIAA Journal, AIAA Paper 2003-4067. https://doi.org/10.2514/6.2003-4067

[6] Yarusevych, S., Sullivan, P. E., & Kawall, J. G. On vortex shedding from an airfoil in low reynolds-number flows. Journal of Fluid Mechanics, Vol. 632, Aug. 2009, pp. 245–271. https://doi.org/10.1017/S0022112009007058

[7] Yuan, W., Xu, H., Khalid, M., & Radespiel, R. A parametric study of LES on laminar-turbulent transitional flows past an airfoil. International Journal of Computational Fluid Dynamics, Vol. 20, No. 1, 2006, pp. 45–54. https://doi.org/10.1080/10618560600578492

[8] Catalano, P., & Tognaccini, R. Turbulence modeling for low-reynolds-number flows. AIAA Journal, Vol. 48, No. 8, 2010, pp. 1673–1685. https://doi.org/10.2514/1.J050067

[9] Catalano, P., & Tognaccini, R. Influence of free-stream turbulence on simulations of laminar separation bubbles. AIAA Journal, AIAA Paper 2009-1471. https://doi.org/10.2514/6.2009-1471

[10] Galbraith, M. C., & Visbal, M. R. Implicit large eddy simulation of low reynolds number flow past the SD 7003 airfoil. AIAA Journal, AIAA Paper 2008-225. https://doi.org/10.2514/6.2008-225

[11] Eppler. R. Airfoil design and data. Springer-Verlag, New York.

[12] Maughmer. M.D. and Somers. D.M. Design and experimental results for a high-altitude long-endurance airfoil." J. Aircraft, Vol. 26. No. 2. 1989. pp. 148-153. https://doi.org/10.2514/3.45736

[13] Nayfeh, A.H., & Ragab. S.A. (1986). Effect of roughness on the stability of boundary layers. AIAA Journal, AIAA Paper 86-1044. https://doi.org/10.1063/1.866815

[14] Somers. D.M. Subsonic natural-laminar-flow airfoils. Springer-Verlag, New York.

[15] Wortmann, F.X. Progress in the design of low drag airfoils. Boundary Layer and Flow Control. G.V. Lachmann (ed.), Pergamon Press. London. 1961, pp. 748-770 https://doi.org/10.1016/B978-1-4832-1323-1.50007-5

[16] Hepperle, M. Turbulators. MH-AeroTools. https://www.mh-aerotools.de/airfoils/turbulat.htm

[17] Mwenegoha H. A., & Jabbal, M. Investigation of passive flow control techniques to enhance the stall characteristics of a microlight aircraft. International Journal of Flow Control. https://doi.org/10.1260/1756-8250.5.3-4.215

[18] Hubber II, A. F., & Mueller, T. J. The effect of trip wire roughness on the performance of the Wortmann FX 63-137 airfoil at low Reynolds numbers. Experiments in Fluids. https://doi.org/10.1007/BF00279740

[19] Lyon, C. A., Selig, M. S., & Broeren, A. P. Boundary layer trips on airfoils at low reynolds numbers. AIAA Journal. https://doi.org/10.2514/6.1997-511

[20] Myers, R. H., Montgomery, D.C. & Anderson-Cook, C. M. Response surface methodology, (4th edn) John Wiley & Sons.

[21] Sevant, N. E., Bloor, M. I. G., & Wilson, M. J. Aerodynamic design of a flying wing using response surface methodology. Journal of Aircraft, 37, 562–569. https://doi.org/10.2514/2.2665

[22] Oh, S. Comparison of a response surface method and artificial neural network in predicting the aerodynamic performance of a wind turbine airfoil and its optimization. Applied Sciences. https://doi.org/10.3390/app10186277

[23] Landman, D., Burnette, D. C., Konuk, E., & E. Baris. Wind tunnel test techniques for low-reynolds number propeller performance enhancement. AIAA AVIATION Forum. https://doi.org/10.2514/6.2022-3641

[24] Montgomery, D. C. Introduction to statistical quality control, (5th edn) Wiley.

[25] Wilcox, D.C. Reassessment of the scale-determining equation for advanced turbulence models. AIAA Journal, vol. 26, no. 11, November 1988. https://doi.org/10.2514/3.10041

[26] Menter, F. R. Two-equation eddy-viscosity turbulence models for engineering applications. AIAA Journal, vol. 32, no. 8. https://doi.org/10.2514/3.12149

[27] Selig, M. S., Donovan, J. F., & Fraser, D. B. Airfoils at low speeds, soarTech Publications, Virginia Beach, VA.

[28] Counsil, J. N.N., & Boulama, k. G. Low-reynolds-number aerodynamics performance of NACA 0012 and Selig-Donovan 7003 airfoils," Journal of Aircraft. https://doi.org/10.2514/1.C031856

[29] Gerakopulos, R., Boutilier, M. S. H., & Yarusevych, S. Aerodynamic characterization of a NACA 0018 airfoil at low reynolds numbers. 40th Fluid Dynamics Conference and Exhibit, AIAA Paper 2010-4629. https://doi.org/10.2514/6.2010-4629

[30] Design Expert, Ver. 12, URL: https://www.statease.com/

[31] Derringer, G., & Suich, R. Simultaneous optimization of several response variables. Journal of Quality Technology, 12:4, 214-219. https://doi.org/10.1080/00224065.1980.11980968